Wear Testing of the HERMeS Thruster

George J. Williams, Jr[1] and James H. Gilland[2]
Ohio Aerospace Institute, Cleveland, Ohio 44142 USA

Peter Y Peterson[3]
Vantage Partners LLC., Cleveland, Ohio 44135 USA

Hani Kamhawi, [4] Wensheng Huang, [5] Drew W. Ahern, [6] John Yim, [7] and Daniel A. Herman[8]
NASA Glenn Research Center, Cleveland, Ohio 44135 USA

and

Richard R. Hofer[9] and Michael Sekerak[10]
NASA Jet Propulsion Laboratory, Pasadena, California, 91109 USA

The Hall-Effect Rocket with Magnetic Shielding (HERMeS) thruster is being developed and tested at NASA GRC and NASA JPL through support of the Space Technology Mission Directorate (STMD) as primary propulsion for the Asteroid Redirect Robotic Mission (ARRM). This thruster is advancing the state-of-the-art of Hall-effect thrusters and is intended to serve as a precursor to higher power systems for human interplanetary exploration. A 2000-hour wear test has been initiated at NASA GRC with the HERMeS Technology Demonstration Unit One and three of four test segments have been completed totaling 728 h of operation. This is the first test of a NASA-designed magnetically shielded thruster to extend beyond 300 hr of continuous operation.

Trends in performance, component wear, thermal design, plume properties, and back-sputtered deposition are discussed for two wear-test segments of 246 h and 360 h. The first incorporated graphite pole covers in an electrical configuration where cathode was electrically connected to thruster body. The second utilized traditional alumina pole covers with the thruster body floating. It was shown that the magnetic shielding in both configurations completely eliminated erosion of the boron nitride discharge channel but resulted in erosion of the inner pole cover. The volumetric erosion rate of the graphite pole covers was roughly 2/3 that of the alumina pole covers and the thruster exhibited slightly better performance. Buildup of back-sputtered carbon on the BN channel at a rate of roughly 1.5 µm/kh is shown to have negligible impact on the performance.

---

[1] Principal Scientist, OAI, Electric Propulsion Systems Branch, 21000 Brookpark Rd., MS 301-3, AIAA Associate Fellow.

[2] Research Team Manager, OAI, Electric Propulsion Systems Branch, 22800Cedar Point Rd., AIAA Associate Fellow.

[3] Senior Engineer, VPL, Electric Propulsion Systems Branch, 21000 Brookpark Rd., MS 301-3, AIAA Senior Member.

[4] Senior Engineer, Electric Propulsion Systems Branch, 21000 Brookpark Rd., MS 301-3, AIAA Associate Fellow.

[5] Engineer, Electric Propulsion Systems Branch, 21000 Brookpark Rd., MS 301-3, AIAA Senior Member.

[6] Engineer, Electric Propulsion Systems Branch, 21000 Brookpark Rd., MS 301-3, AIAA Member.

[7] Engineer, Electric Propulsion Systems Branch, 21000 Brookpark Rd., MS 301-3, AIAA Senior Member.

[8] Senior Engineer, Electric Propulsion Systems Branch, 21000 Brookpark Rd., MS 301-3, AIAA Associate Fellow.

[9] Technical Group Lead, Electric Propulsion Group, 4800 Oak Grove Dr., MS 125-109, AIAA Associate Fellow.

[10] Senior Engineer, Electric Propulsion Group, 4800 Oak Grove Dr., MS 125-109, AIAA Senior Member.

I. Introduction

For missions beyond low Earth orbit, spacecraft size and mass can be dominated by onboard chemical propulsion systems and propellants that may constitute more than 50 percent of the spacecraft mass. This impact can be substantially reduced through the utilization of Solar Electric Propulsion (SEP) due to its substantially higher specific impulse. Studies performed for NASA's Human Exploration and Operations Mission Directorate and Science Mission Directorate have demonstrated that a 50kW-class SEP capability can be enabling for both near term and future architectures and science missions.[1] To enable SEP missions at the power levels required for these applications, an in-space demonstration of an operational 50-kW-class SEP spacecraft has been proposed as an SEP Technology Demonstration Mission (TDM). In 2010 NASA's Space Technology Mission Directorate (STMD) began developing large, deployable photovoltaic solar array structures for high-power electrical power production and high-power electric propulsion technologies.[2,3,4] The maturation of these critical technologies has made mission concepts utilizing high-power SEP viable.

The Asteroid Redirect Robotic Mission (ARRM) is the leading candidate SEP TDM concept that utilizes an SEP spacecraft to return up to 20 metric tons (up to 6 m maximum extent) of asteroidal mass from the surface of a larger asteroid, to a stable orbit around the Moon for subsequent access by a human crewed mission.[5,6,7] The Ion Propulsion System (IPS) for ARRM will be used for heliocentric transfer from Earth to the target asteroid, orbit capture at the asteroid, transfer to a low orbit about the asteroid, a planetary defense demonstration after retrieval of the asteroidal mass from the larger asteroid, departure and escape from the asteroid, the heliocentric transfer from the asteroid to lunar orbit, and insertion into a lunar distant retrograde orbit. In addition, the IPS will provide pitch and yaw control of the spacecraft during IPS thrusting. To date, the technology development, performed by the NASA Glenn Research Center (GRC) and the Jet Propulsion Laboratory (JPL), has been focused on an in-house effort to mature the high-power Hall thruster and power processing designs. This work has recently begun the transition to a commercial vendor for the development of an Engineering Development Unit (EDU) EP string and optional Qualification Model (QM) and Flight Model (FM) hardware delivery in a timeline consistent with the current ARRM implementation. The flight electric propulsion string hardware will be provided as government furnished equipment to the Asteroid Redirect Vehicle (ARV) prime contractor.

Erosion of the boron-nitride (BN) insulators in the discharge channel has been the primary service life limiter of Hall-effect thrusters (HETs) and, in addition to limits on the available in-space power, has precluded its use as primary propulsion on most NASA missions. Magnetic shielding has been explored in recent years as a breakthrough approach to mitigate this erosion,[8] resulting in laboratory demonstration of the expected reduction of the erosion rates in 6-kW and 20-kW Hall thrusters.[9,10] Knowledge gained from applying magnetic shielding circuit design in these two Hall thrusters was leveraged in the design and construction of a new 12.5-kW Hall thruster.[11] The effort has generated the Hall-Effect Rocket with Magnetic Shielding (HERMeS) thruster which is intended to provide a baseline for the primary propulsion for ARRM.[12,13] The HERMeS Technology Demonstration Unit (TDU) has reached the level of maturity where a series of higher fidelity tests including environmental testing and wear testing are required for further development.

Wear testing of HERMeS has four objectives:

- Quantify wear trends over an extended period of thruster operation to identify unknown failure modes and support validation of service-life models
- Quantify performance trends over an extended period of thruster operation to also identify unknown failure modes and support validation of service-life models
- Quantify the deposition rate of back-sputtered facility material to identify the impact of this deposition on thruster surfaces, to validate facility modeling and to inform the facility configuration for future tests
- Provide guidance for future long-duration testing by identifying best practices and unknown issues associated with facility operation and configuration.

Wear testing has progressed in distinct segments over the first 730 h of a 2000 h test. As discussed below, each segment had specific sub-objectives associated with the particulars of the stages. The first segment characterized the overall performance of the thruster which had incorporated several changes that resulted from the previous testing in 2015. A thorough discussion of the results of this testing including comparisons with the previous data are presented in a companion paper.[14] The next two segments characterized the wear, facility back-sputter and performance associated with two options for the thruster configuration. The performance and wear trends observed in these two segments are presented and discussed below. Back-sputter trends and performance characterization outside of the wear test point are discussed in companion papers.[14,15] The wear testing has entered its fourth segment, which is an extended duration test to 2000 h of total operation.

American Institute of Aeronautics and Astronautics

II. Test Configuration

The HERMeS thruster was operated in Vacuum Facility 5 (VF-5) at NASA GRC. VF-5 utilized cryogenic surfaces to maintain a pressure near the thruster less than $3 \cdot 10^{-5}$ Torr (corrected for Xe) during full power operation of the thruster. The test setup included a laboratory propellant feed system and power console, an inverted pendulum thrust stand, a data acquisition system, and several physical probes for plume interrogation.

A. Thruster

The HERMeS Technology Demonstration Unit One (TDU-1) underwent extensive performance testing during 2015.[16] Figure 1 shows a photograph of the TDU with graphite pole covers during wear testing. The pole covers protect the downstream surfaces of the inner and outer magnetic pole pieces from eroding ion impingement. Photographs of the various configurations associated with each segment of the test campaign are given in Table 1. The thruster demonstrated nominal performance, incorporated a series of minor design modifications, and provided data which were correlated with detailed plasma modeling of the near-field plume. Experimental data was used to anchor structural and thermal modeling results. As a result, there is high-confidence that a TDU-based design will meet ARRM thruster requirements.

Entering the wear testing, several changes were incorporated into the thruster including an improved anode manifold mechanical fastening scheme, new inner electromagnet coil, and new BN discharge channel. As discussed in more detail below in Section III-C, three sets of pole covers were incorporated, unique to each test segment. Graphite inner and outer pole covers were base-lined and incorporated in the first two segments of the wear testing. Alumina pole covers were used in the third segment. (BN pole covers were used during previous HERMeS testing.)

The thruster incorporates a laboratory model hollow cathode assembly (HCA) with graphite keeper. The HCA heavily leverages the configuration used successfully for 52,000 hr as the discharge cathode in the NASA Evolutionary Xenon Thruster (NEXT) Long Duration Test.[17] It is also very similar to the HCA used during previous HERMeS testing.

Figure 1. TDU-1 with graphite pole covers operating in VF-5 during Segment II of testing.

B. Support Hardware

For the HERMeS TDU-1 test campaign the thruster was powered with a laboratory power rack that contained the discharge, inner and outer electromagnet, cathode heater, and cathode keeper power supplies. The discharge power supply consists of three 15 kW (1000 V and 15 A) power supplies that were connected in a master-slave configuration. A computer was used to sweep the thruster discharge voltage during the thruster stability characterization test.[14]

The data acquisition system used for the TDU-1 electrical configuration characterization was a multiplexed datalogger with computer interface. The datalogger monitored the voltages, currents, temperatures, propellant flow rates, chamber pressure, and thrust every second during performance testing. The computer interface had the additional benefit of allowing a number of monitored channels to be monitored with failsafe limits for unattended operation. The uncertainties of the datalogger measurements were ±0.05% for the voltage and current measurements.

A laboratory propellant feed system was used in the TDU-1 test campaign. The feed system supplied xenon to the thruster and was also used to elevate the facility background pressure. The propellant feed system utilized four mass flow controllers (MFC). A 500 and a 100 sccm MFC supplied xenon propellant to the thruster and cathode, respectively. A 200 and 1,000 sccm MFC supplied xenon to elevate the facility pressure. The MFC calibration curves indicated that the anode and cathode flow rate uncertainties are ≤1% of set values.

The performance characterization of the TDU-1 Hall thruster was measured with an inverted pendulum null-type thrust stand. The NASA GRC high-power thrust stand has an accuracy of ≤1% based on a statistical analysis of the calibration and thrust zero data taken throughout the test campaign. The high-power thrust stand was operated in a null-type configuration, which allows the thruster to remain stationary while testing. The thrust stand was also equipped with a closed loop inclination control circuit, which utilized a piezoelectric element to minimize thermal drift during performance testing. The thrust stand was calibrated in-situ with calibrated masses on a pulley system connected to a stepper motor. The thrust stand was calibrated before and after each performance mapping period.
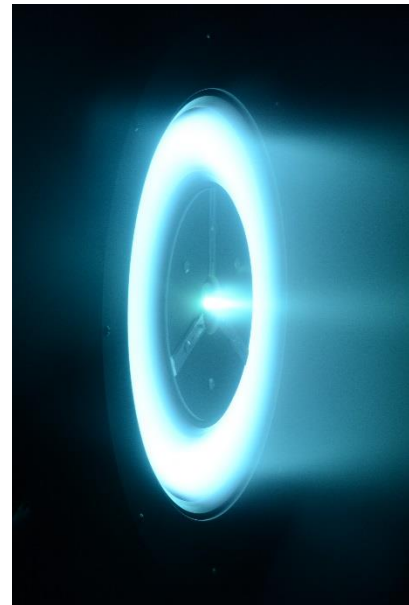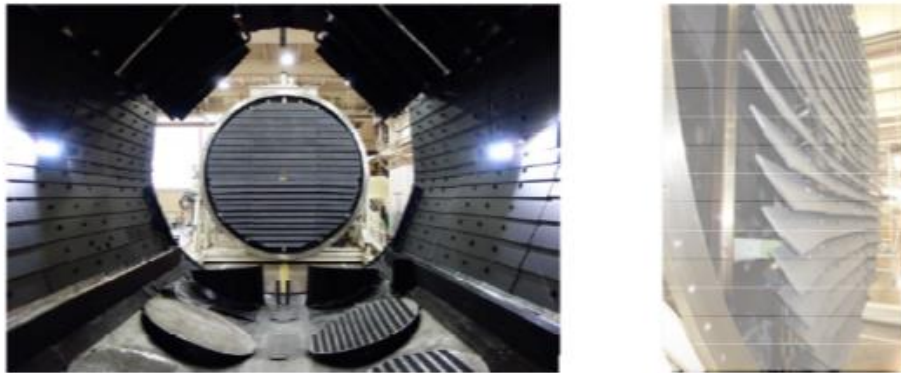
Figure 2. Graphite paneling in VF-5. The beam target with angled plates is shown to the right.

C. Vacuum Facility

Vacuum Facility 5 was reconfigured in 2015 in part to provide more uniform pumping and reduced plume divergence caused by charge exchange collisions. This configuration was used successfully for performance characterization of HERMeS. Prior to this characterization testing, the beam target and the surfaces of the chamber downstream of the thrust stand were covered in graphite plate to preclude plume-ion impact of all nitrogen-cooled and metal surfaces. Figure 2 shows a photograph of the chamber as viewed from the thruster. As discussed by Gilland, this plating resulted in a four-fold reduction in back-sputter rate from the configuration testing with HERMeS in 2015.[15] Figure 3 shows a schematic of VF-5 with the location of the pumping surfaces behind (west) and downstream (east) of the thrust stand.

All metal surfaces within 1-m of the thruster were electrically isolated from ground to mitigate facility coupling effects. All windows were fitted with mechanical shutters. However, no changes to the pumping configuration were incorporated from previous testing save those through normal maintenance.

Health monitors (pressure, temperatures, and on/off status) on various facility components were tied to the DAQ/power interlock to provide maximum protection of the thruster.
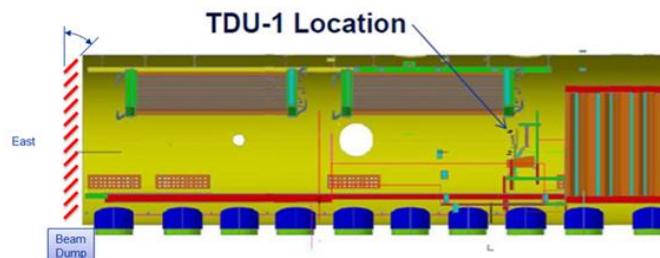

Figure 3. A schematic of VF-5 showing the location of the thruster (TDU-1) relative to the pumping surfaces.
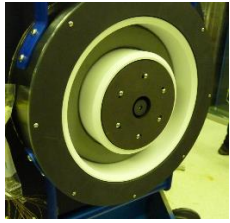
D. Diagnostics

Diagnostics include a plasma probe rake, internal cameras, quartz-crystal microbalances (QCM), witness plates, ion gauges, a residual gas analyzer, and externally mounted cameras (including an infrared imaging camera). The plasma probes include a retarding potential analyzer (RPA), Faraday probe, Langmuir probe, and Wein (ExB) filter. These are identical to those used during previous testing and are rotated through the plume via an r-θ stage mounted above the thruster. Three QCMs located within 1-m of the thruster at different clocked positions monitor back-sputter rates. All of these diagnostics are monitored and recorded via computers separate from the DAQ, which are time-synchronized with the DAQ.

Optical emission spectroscopy (OES) was incorporated via an in situ optical probe. The probe was connected via fiber optic cable to three spectrometers on the outside of VF-5. For all segments of the test, the probe's collection volume was focused on the outer edge of the inner front pole where masks transitioned to the inner pole cover. The spectra was recorded periodically during all segments of the wear test.

American Institute of Aeronautics and Astronautics

Table 1. Correlation of Test Objectives with Measurement Methodology.

Objective/metric	Category	Measurement	Measurement Method	When
Quantify wear trends				
Component erosion	Primary	Surface height profile	Optical profilometry	Pre/post-test (pre/post-test segment)
Anomalous (visible) erosion	Primary	Digital images of TDU surfaces	Digital cameras	On-demand
Real-time assessment of B & C fluxes	Secondary	Relative density of sputtered atoms	Optical emission spectra	On-demand
Cathode depletion	Secondary	Weight of insert	High-resolution balance	Pre/post-test
Thermal deformation	Primary	Orifice Plate Temperature	Thermocouple	Continuous
		TDU component temperatures	Thermocouple	Continuous
Emitter temperature	Secondary	HCA orifice plate temperature	Thermocouple	Continuous
Quantify performance trends				
Nominal Operating Point	Primary	Thrust	Calibrated thrust stand	Continuous
		Flow rate	Calibrated flow meters	Continuous
		Currents and Voltages	Calibrated shunts and probes	Continuous
		Thruster Telemetry (stability)	IVB sweep	At regular intervals
Ref. Operating Points	Primary	*As with nominal point*	*As with nominal point*	At regular intervals
Plume characterization	Primary	Ion current density	Faraday probe on probe arm	At regular intervals
		Ion energy distribution	RPA on probe arm	At regular intervals
		Electron Temp. & Plasma Pot.	Langmuir probe on probe arm	At regular intervals
		Charge-dependent current flux	ExB probe on probe arm	At regular intervals
Thermal trends	Primary	TDU component temps	Thermocouples	Continuous
	Tertiary	Anode and BN surface temps	IR camera	On demand
HCA emitter Temperature	Secondary	HCA orifice plate temperature	Thermocouple	Continuous
HCA insert health	Primary	Keeper IV trace for 3 mass flows	IV trace	At regular intervals
HCA plume mode onset	Tertiary	A/C component of keeper voltage	IV trace	At regular intervals
TDU plume structure	Tertiary	Plume structure of Xe I and Xe II	Single-frequency images	On demand
Quantify back-sputter				
Back-sputter rate	Primary	Mass of back-sputtered deposition	QCM	Continuous
Back-sputter composition	Primary	Mass-spec of deposition	SEM / XDAS	Post-test
Spatially resolved sputter yields	Secondary	Thickness and composition of BSM	Witness plates	Post-test/post-test segment
Provide guidance for future HET tests				
Mature test procedures	Primary	Effectiveness of procedures / plans	Degree of modification	Continuous
Characterize onset of maximum cryo loading	Secondary	Pressure trends	Calibrated ion gauges	Continuous
Minimize spalling during regens	Secondary	Degree of spalling	Inspection via camera	Periodic

American Institute of Aeronautics and Astronautics

Table 2. Summary of the test segments of the TDU-1 wear test.

Test Segment	I	II	III	IV (planned)
Objective particular to the Segment	Measure TDU performance with graphite pole covers	Measure erosion of graphite pole covers,	Measure erosion and performance with Al_2O_3 pole covers	Measure erosion and performance over an extended period
Image				
Inner Pole Cover Configuration	Graphite, no masks, for 100 h No cover for 22 h	Polished graphite with Mo masks	Alumina with alumina masks	Same pole cover as Segment II with graphite masks
Outer Pole Cover Configuration	Graphite, no masks, for 100 h No cover for 22 h	Same pole cover as segment I	Alumina with no masks	New, polished graphite with graphite masks
Electrical Configuration	Varied	Cathode-tied	Floating	Cathode-tied
Duration, h	122	246	360	~1272
Time-on-HCA and BN at end of segment, h	122	368	728	~2000

III. Approach

Table 1 provides a correlation of the broad objectives of the wear testing with the various diagnostics and test telemetry. Characterizations categorized as primary are crucial to the evaluation of the TDU design and to the preparations for follow-on testing. In general, measurement of HCA health and wear would be classified as primary objectives. However, because the hollow cathode assembly is of lower fidelity than the TDU-1 thruster, its characterization is deemed to be secondary. Tertiary objectives reflect measurements that have the potential to support modeling efforts but are not critical to the evaluation of the TDU or its performance.

As mentioned in Section I, the wear test campaign has been divided into four segments, three of which have been completed. Table 2 summarizes the particular objectives, configurations, and durations of the different segments. The wear test operating point was defined as 600 V, 12.5 kW. Testing in Segment I led to definition of the magnetic fields and flow rates for the wear test points which varied slightly with thruster electrical configuration.[22]

A. Quantification of Wear Trends

Erosion trends were quantified through three mechanisms including in-situ (atmospheric) optical profilometry, component profilometry via non-contact bench top profilometry, and optical emission spectroscopy. Magnetic shielding was successfully incorporated into the TDU's design to eliminate erosion of the BN discharge chamber.[12] This erosion has historically been the life-limiting wear mechanism for Hall-effect thrusters and its removal has introduced or highlighted other sources of potential failure. In particular, erosion of the inner front pole cover may expose the pole to the ambient plasma. This has been identified as the primary failure mechanism entering the wear test. In addition to verifying the BN does not erode and quantifying the erosion of the pole covers, erosion of the cathode keeper or cathode orifice plate may occur. To enable absolute wear measurements, reference surfaces not subject to erosion or deposition are required. For the in-situ profilometer, this surface is provided by a detachable reference surface. However, for the bench top profilometer, masks are incorporated.

American Institute of Aeronautics and Astronautics

During the majority of the first segment of the test campaign, graphite pole covers were incorporated and the thruster body was electrically connected to the cathode to minimize the erosion. However, because the extended performance testing requires operating the thruster over a wide range of operating conditions, including extended operation in different electrical configurations, wear rates and patterns are of limited value. As the second segment the wear campaign, a 246 h wear test was undertaken with a modified graphite inner pole cover to facilitate quantification of the erosion (and perhaps deposition) rates. The pole cover was polished such that the surface roughness was on the order of a few microns. As shown in Fig. 4, three molybdenum (Mo) strips were placed at 0 (twelve o'clock), 120 and 240 degree azimuthal locations. Each Mo strip itself had two thin Mo masks spot-welded to its surface. Thus, the protected graphite surface provided a pre-test reference for the remainder of the pole cover and, if the erosion rates proved small, the Mo strips provided a pre-test reference for the remainder of the Mo masks. This procedure was used successfully by Sekerak in 2015.[18]
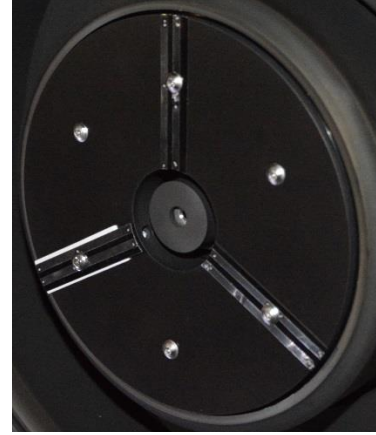

Figure 4. Graphite inner pole cover with Mo masks.

Because the wear-predicting models associated with the TDU had not been validated with test data, a large uncertainty remained after the selection of graphite as the pole cover material as to whether it was either a) needed to meet service life requirements or b) trading one issue for another (associated with conducting pole covers). Therefore, a second short duration wear test with alumina pole covers was undertaken as the third segment of the test campaign. Three alumina masks were incorporated at the same azimuthal locations as the Mo masks on the alumina inner pole cover. Use of Mo masks for the alumina test would have introduced ambiguity as the Mo would have significantly altered the electric field at the face of the alumina.

Wear of the BN channel and of the cathode keeper and that of the pole covers was characterized before and after each test segment through use of the in-situ profilometer. This device has resolution on the order of 10 μm as opposed to ~1 μm with the bench top profilometer. However, the convenience of maintaining the fidelity of the test configuration and the importance of staying beneath the detection threshold of the in-situ device made this technique of great value.

Optical emission spectroscopy was incorporated as a real-time, relative measurement technique following the procedures outlined in Williams.[19] Boron atoms have been correlated with BN erosion rates.[19,20] Neutral aluminum and oxygen atoms have been correlated with alumina (Al_2O_3) erosion.[21] Molybdenum and carbon atoms also lend themselves to OES, though all of these are subject to masking by the emission of various xenon atom and ion transitions. As a first approximation, the OES signal strengths of these sputtered atoms are normalized to the OES signal strengths of nearby xenon emission lines. While day to day settings of the spectrometer were maintained constant, slight variations (and variations from potential fouling of the collection optics) were removed by self-normalizing the OES signals as well as normalizing them to xenon. For instance, for five Mo measurements made over the course of the second test segment, each normalized Mo OES signal is:

$$I_{Mo,i} = \frac{S_{Mo,i}/S_{Mo,max}}{\sum_{j=1}^{3} S_{Xe,i,j}/\sum_{j=1}^{3} S_{Xe,max,j}}$$

where S is the measured OES signal strength at a given wavelength.

B. Quantification of Performance Trends

Because the TDU incorporated a large number of changes suggested by the performance testing in 2015,[11] more testing to characterize performance was required than is normally associated with a wear test campaign. An extensive period (100+ h) of performance characterization was undertaken at the onset of the wear test to compare the TDU performance to previous test entries and to determine the nominal operating point for the wear test. This testing included extensive stability and sensitivity testing. The results of this segment of the testing are given in Kamhawi.[14]

Given the nominal operating point, periodic performance testing at several other TDU operating points was also undertaken during the wear testing to quantify changes induced by extended operation. These changes may result

American Institute of Aeronautics and Astronautics

from thermal fatigue, erosion, deposition, or simply the removal of impurities in the insulators or other components of the thruster. Particular reference firing conditions were repeated to characterize these changes.

Plume mapping was minimized following the initial performance characterization in Segment I to minimize the flux of back-sputtered material onto the thruster as the probes were swept through the plume. However, plume characterization at the wear test operating point was undertaken more frequently (roughly every 250 h) to determine if there is a significant change in the thruster's operation.

C. Quantification of Facility Back-sputter

Back-sputtered material has the potential to render results of the wear testing ambiguous or misleading by modifying surfaces in ways inconsistent with operation in space. In particular, conductive films may electrically short otherwise isolated components, thick films may spall or induce thermal stresses in dielectrics, and back-sputtered material may mask or significantly alter the erosion of thruster surfaces exposed to ion fluxes. Three quartz crystal microbalances (QCMs) and two boron-nitride witness surfaces are located in the exit plane of the thruster to provide rate measurements and surface morphology of the back-sputtered flux, respectively. Witness plates are also located throughout the vacuum chamber to facilitate validation of back-sputter models based on plume impingement. A detailed discussion of the measurements and numerical prediction of the back-flux within VF-5 is given by Gilland.[15]

D. Guidance for Future Testing

Guidance for future testing includes several facility related procedures as well as lessons learned through conducting the test itself. In particular, alerts and alarms associated with various facility processes are being assessed as appropriate shutdown criteria for the TDU in unattended operation.

Also, since its reconfiguration, no testing in VF-5 has processed sufficient xenon to reduce its pumping speed or induce pressure spikes through the shedding of frozen xenon from the cryopump surfaces. It is estimated that over 700 h of continuous operation at the TDU wear test operating point is required to reach this point. The long duration portion of this test campaign should surpass this estimated limit and the behavior of the facility will be characterized to facilitate the scheduling of cryopump regeneration.

IV. Results

The following discussion concentrates on the results of the two wear test segments of the test campaign as they pertain to the overall wear test objectives. A thorough review of the performance and plume characterization of the TDU is given by Kamhawi.[14]   Following some general comments on the conduct of the test and the BN discharge chamber, the performance trends of segments I, II and III will be discussed together with emphasis being placed on variations within each of the latter two. The wear associated with the graphite and alumina inner pole covers and with the cathode keeper will be discussed separately.   Lack of wear of the BN discharge chamber will be discussed with trends in back-sputtered material.

Only two significant interruptions to the test campaign occurred. One was attributed to a leak in the cooling water supply, which posed no risk to the test hardware as the thruster was shut off by interlock hours before the cryogenic cooling was interrupted. The other was caused by a short in one of the power feedthroughs to the chamber which required venting to repair. Repeated intentional interruption of the testing to change TDU configuration makes calculation of the overall duty cycle problematic, but unintended shutdowns during the wear testing accounted for less than 15% of the total test time.

A. Trends in Thruster Performance

In general, there were no significant variations in thruster performance over the course of each of the wear test segments.   The segments did exhibit differences, with the configuration of Segments I and II (thruster body tied to cathode and graphite pole covers) yielding higher performance. While this is
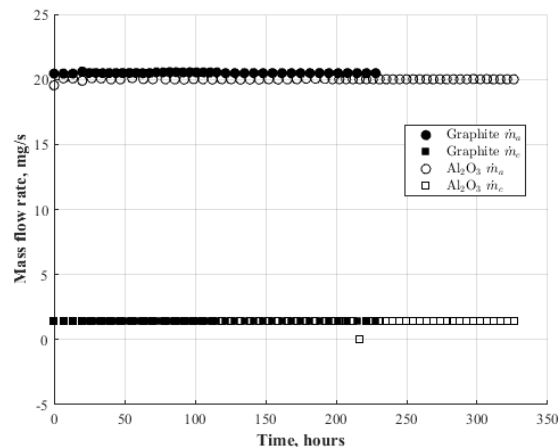

Figure 5. Flow rate as a function of time for the two wear test segments.

8

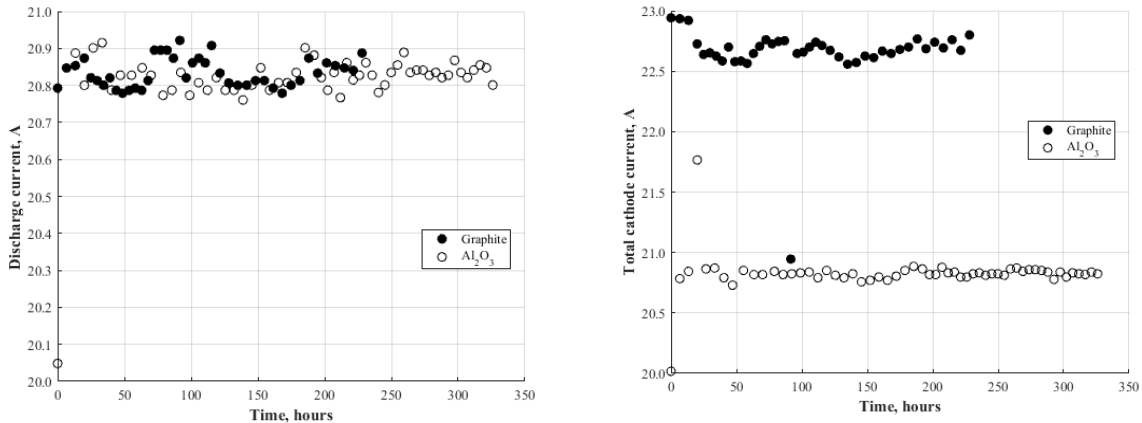American Institute of Aeronautics and Astronautics

Figure 6. Comparison of trends of discharge current (left) with total cathode current (right) with time over the two wear test segments.

extremely relevant to the go-forward plan for the TDU, it is somewhat incidental to the objectives of the wear testing itself which is intended to reveal temporal changes. Discussion of the relative trends is given in Kamhawi.[14] The following discussion assumes 12.5 kW, 600 V operation unless otherwise stated.

For a given thruster configuration, the discharge current was maintained constant through variation of the flow rate. Figure 5 shows that there was negligible variation in flow rate for both wear test segments. For convenience, all data associated with the wear test segment utilizing graphite pole covers is referred to as "Graphite". Similarly, all data associated with the segment utilizing alumina pole covers is referred to as "Al_2O_3".

Figure 6 compares the trends in discharge current and total current for the two configurations. Note that the total current differs by the current collected by the thruster body flowing from the ambient plasma through the cathode to the plasma near the discharge. For the floating configuration, this current was identically zero and the total cathode current and the discharge current were identical. For the cathode tied configuration, this current was 1.8 A. Figure 7 shows that there was roughly a 1 % variation (constant within the uncertainty of the measurements) in thrust over these segments, but that the thrust differed by over 3% between the two configurations.

With the exception of occasional performance testing, the magnet currents were maintained at constant values after roughly hour 20 of the graphite wear test. The first 20 h of the graphite wear test were at a slightly higher field strength. Figure 8 shows variations in the magnet voltages. Note the higher voltages at the higher currents/field strengths, the higher voltages for the Al_2O_3 test, the crossing of the voltages shortly into the Al_2O_3 test and the slight divergence thereafter. These are the only secular trends observed
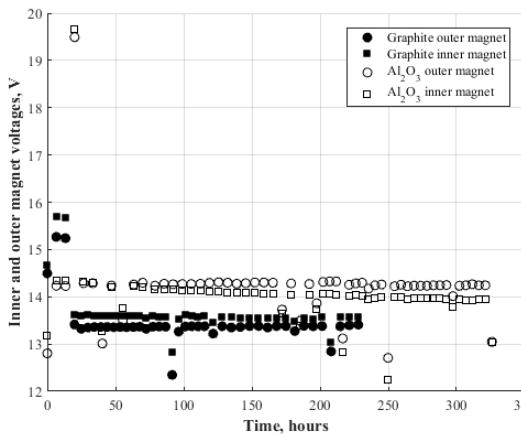

Figure 8. Variations in the magnet voltages as a function of time for the two wear test segments.
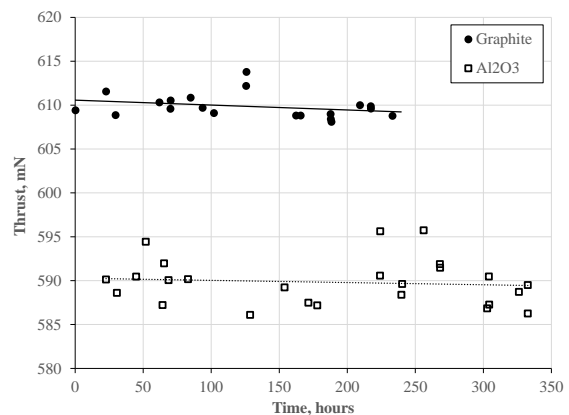

Figure 7. Thrust as a function of time for the two wear test segments.
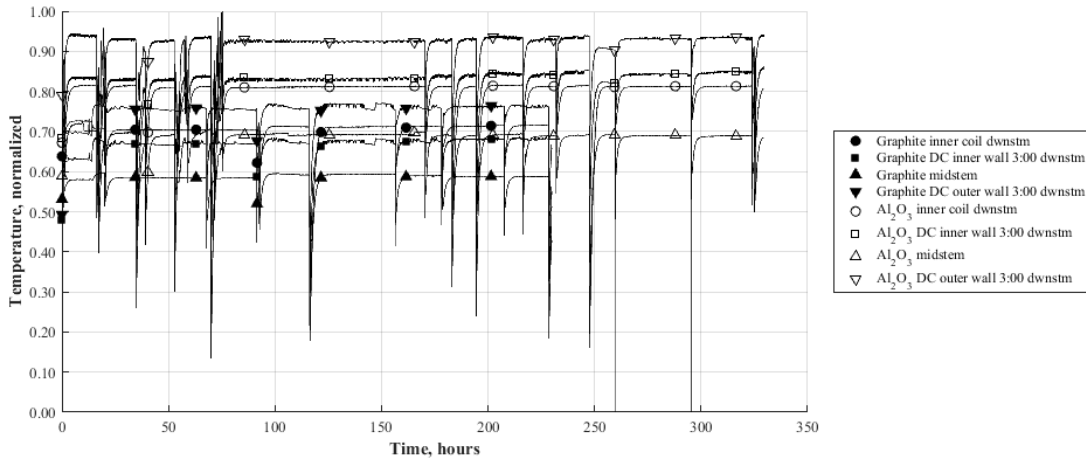
9

American Institute of Aeronautics and Astronautics

Figure 9. Variations in the selected temperatures as a function of time for the two wear test segments. The temperatures are normalized to the maximum temperature which was reached around 70 h of Segment II during throttling.

and they appear to be within expectations.[14] Coupling voltages, thruster body to ground voltages, and the peak-to-peak variations of these voltages remained constant throughout each wear test segment.

Figure 9 compares the temperatures at four locations in the thruster as a function of time over the two wear test segments. The values are normalized to the maximum within the data set across both test segments (marker not shown). The temperatures of the alumina configuration are clearly higher than those of the graphite configuration. The inner wall of the discharge channel is cooler than the inner coil at their downstream ends for the graphite configuration but not for the alumina one. This is likely a result of the thermal conductance at the pole covers. However, more importantly for wear testing, note that there is no significant variation in the individual temperatures over the course of each test. Note also that the temperatures return to the same values following periodic cool-downs associated with thruster shutoffs. This suggests that the thruster is operating in thermal steady state and that there are no significant changes due to fatigue or deposition over these relatively short test durations.

Throughout the test campaign, reference firing conditions have been revisited to assess the impact of wear and deposition on TDU performance. However, these were not defined until the end of the performance (first) segment of the campaign. Figure 10 compares trends in thrust for three power settings with a discharge current of 20.8 A. Note that the performance over the course of each wear test segment is constant. For the lower powers/voltages, the performance for the two configurations is indistinguishable with efficiencies of 61% and 65 % for 300 V and 400 V,
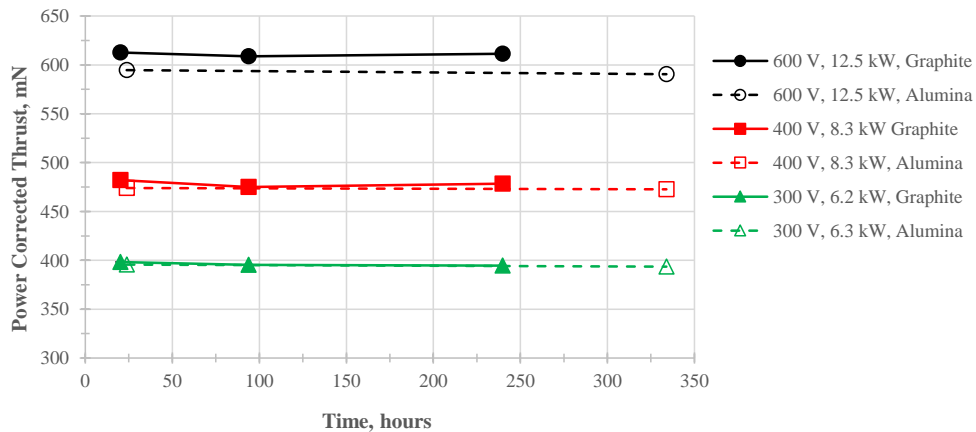

Figure 10. Variations power-corrected thrust for three thruster operating conditions over time during each of the two wear test segments.

10

American Institute of Aeronautics and Astronautics

respectively. There is, however, a 2.5% improvement in efficiency for the graphite, cathode-tied configuration at the wear test operating point of 600 V, 12.5 kW. More thorough discussions of these trends are provided in companion papers by Kamhawi[14] and Peterson.[22]

Plume characterization consisting of Faraday probe sweeps, and discrete RPA, ExB, and Langmuir probe measurements were made at the beginning and ending of each wear test segment. These measurements showed no changes in the plume over the course of each segment. As discussed in Kamhawi[14] and Peterson,[22] the graphite, cathode-tied configuration is slightly (0.5 deg) more divergent with high-energy ions present up to 75 deg from thruster centerline. For the alumina, floating configuration, high-energy ions are confined within 60 deg from centerline.

B. Discharge Channel Wear/Deposition

No wear of the BN discharge channel was observed during the 728 h of operation indicating that the discharge channel is completely shielded by the magnetic field. After roughly 50 h of operation with graphite pole covers during the Segment I of the wear test the BN became dark (black). This change can be seen in the first two images in Table 2. No corresponding change in thruster performance was observed. No samples from the discharge chamber have been taken. Surface resistance measurements after 728 h showed an average point-to-point resistance on the surface of 35 Ω. Anode to channel resistance was 10s of kΩ after 728 h.

Figure 11. Comparison of a BN wafer before (left) and after (right) Segment III of the wear test.

In an attempt to indirectly assess whether the darkening of the discharge channel was due simply to back-sputtered carbon or to a more complex thermo-chemical reaction of the BN itself, a BN witness plate was placed roughly 5 cm radially outward from the thruster body, in front of the thruster's radiator and facing downstream during Segment III of the wear test campaign. Figure 11 shows the BN wafer before and after the 360 h segment. To the eye, its discoloration is identical to that of the BN discharge chamber. Optical profilometry and scanning-electron microscopy (SEM) both show a film thickness less than 1 μm, and the SEM indicated that the film was almost entirely composed of carbon. This suggests that the darkening of the discharge chamber is due primarily to back-sputtered material. As discussed below, the thickness of the film is consistent with the measured back-sputtered rate.
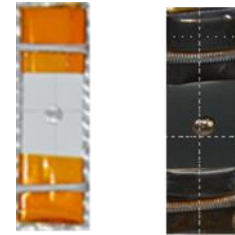
C. Inner Front Pole Covers

Erosion patterns on the graphite and alumina inner front pole covers differ significantly. Figure 12 shows the measured erosion rate as a function of normalized inner pole cover radius for the graphite pole cover for three azimuthal locations. Note that the rate minimizes near the mid-radius and reaches maxima near the edges. The three measurements were made by comparing the surface masked by the Mo strips to the exposed surface within several millimeters of the strips. Negligible azimuthal variation in the exposed surface between the strips was measured.
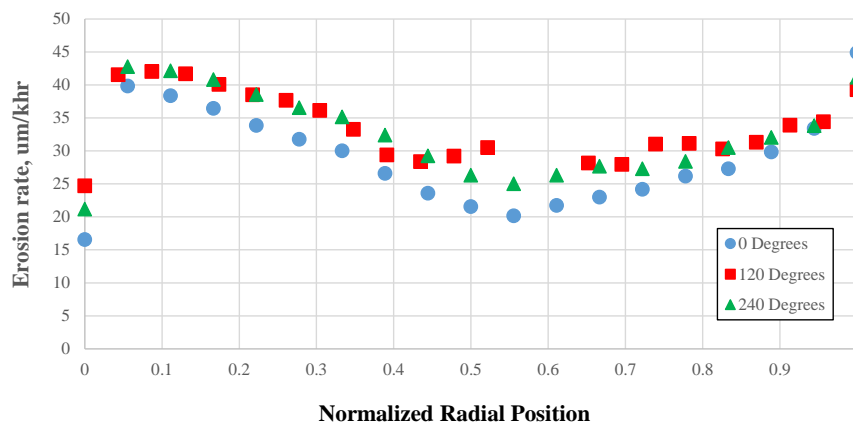

Figure 12. Erosion rates of the graphite inner pole cover as a function of radial location for three azimuthal locations. A radial position of zero is nearest the cathode.

11
American Institute of Aeronautics and Astronautics

The Mo strips themselves experienced significant erosion in a pattern that appears consistent with that observed on the graphite pole cover. An electrical short in a vacuum feed thru that occurred 101 h into Segment II required venting of the vacuum chamber. This fortuitously allowed replacement of one of the Mo strips with another. This replacement was necessary because the erosion near the ends of the Mo strips had removed the spot-welds and was thus exposing the entire Mo strip and precluded a calibrated measurement. Figure 13 shows the calculated rates based on the measured erosion of the two different masks attached at the 120-degree location. The highest uncertainty occurs at the ends where the erosion was the greatest.
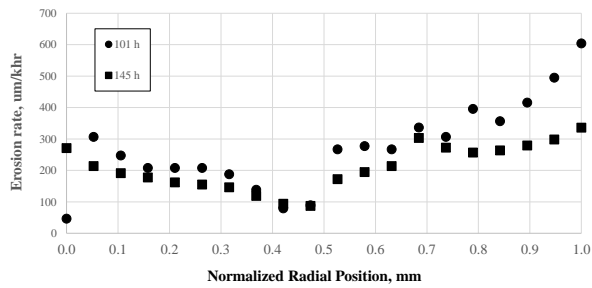

Figure 13. Erosion rates of the Mo witness plate on the graphite inner pole cover as a function of radial location as a function of time for two time periods of Segment II.
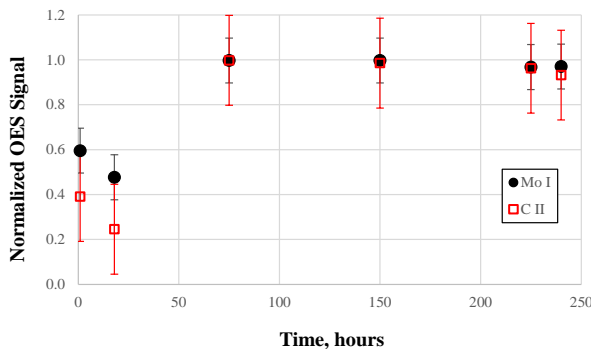
Normalized optical emission spectra for C II at 426.9 nm, and Mo I at 380.0 nm are shown in Fig. 14. Note that both signals show a jump between 20 and 75 h (discrete points of OES data collection). This discontinuity roughly coincides with the decrease in magnetic field strength shown by the decrease in magnet voltages in Fig. 8. The OES data suggest that the erosion rate was roughly constant after this point which is consistent with the majority of the data shown in Fig. 13. Because the OES data are relative, there was no quantitative correlation between the Mo and C rates or between the two levels within each trend. Unfortunately, OES data were only collected at one radial position because of a failure in a second fiber optic feedthrough.

Figure 15 shows the erosion rates calculated for the erosion measured on the alumina inner pole cover.

Figure 14. Variations OES signals for Mo and C near the outer radius of the inner pole cover during Segment II.

As in Fig. 12, rates are shown for three azimuthal locations and the depths are measured with respect to the surface protected by the masks. Over the inner 40% of the pole cover, the rates are similar between alumina and graphite. However the rate was significantly higher over the outer 60% for the alumina. The maximum rate is roughly four
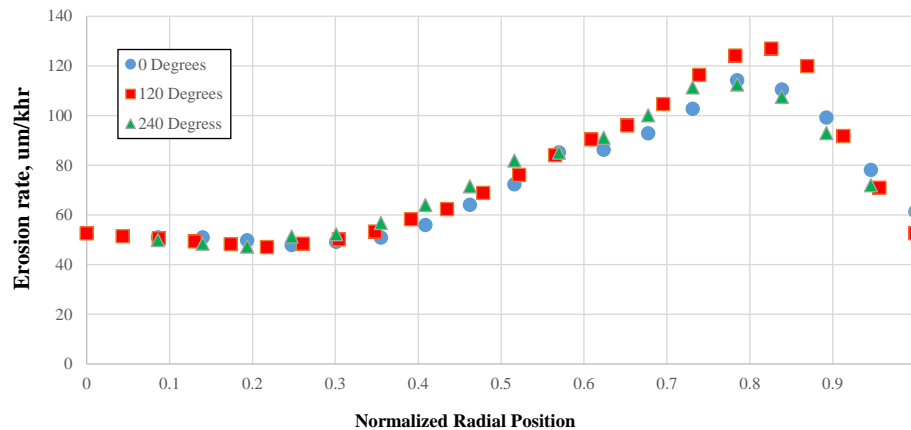

Figure 15. Erosion rates of the alumina inner pole cover as a function of radial location for three azimuthal locations. A radial position of zero is nearest the cathode.

12

American Institute of Aeronautics and Astronautics

times that measured on the graphite pole cover. As with the graphite pole cover, no azimuthal variation was measured between the masks.

Figure 16 shows OES Al I-394.5 nm data at discrete times during Segment III of the wear test. Alumina has been shown to emit at this aluminum neutral transition and at oxygen, O I, 420.2 nm.[21] However, the O I line was obscured by Xe II spectra. Within the uncertainty, the erosion appears to be constant over the test segment.
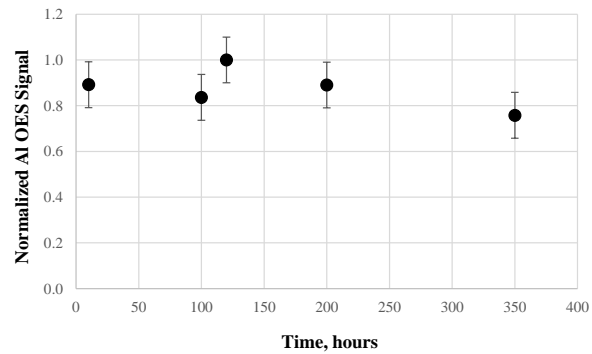
D. Outer Front Pole Covers

The graphite outer front pole cover appears to have a small groove eroded azimuthally just outside of the mounting hole pattern. The rate is estimated at 44 µm/kh over a radial width of 1.5 mm. However,

Figure 16. Variations OES signals for Al near the outer radius of the inner pole cover during Segment III.

because the outer pole cover has a rough, unpolished surface, the uncertainty in this measurement is very high, up to 50%. Uncertainty is increased because the reference surface for this measurement is the outer pole surface as measured through the hole pattern. The pole covers were removed without the thruster and, thus, without this reference. However, the groove was not detected during pre-test scans.

A similar lack of reference existed for the alumina outer pole cover. Machine mark patterns consistent with pre-test measurements were still clearly visible and there were no other distinguishing characteristics found during post-test inspection. This suggests that any erosion would have been uniform across the cover's surface. As with the inner pole cover, no deposition was noted, which suggests some surface removal may be occurring. However, since there was no distinguishable markings, no rate can be determined. In-situ profilometry suggested any changes in the surface of the outer pole covers were less than the detection limit of the device.

E. Hollow Cathode

The hollow cathode was ignited 87 times over the course of the test campaign. These included regular zero-thrust measurements to track thrust stand drift, restarts of the thruster following configuration changes and unscheduled shutdowns, restarts during the initial performance mapping and during occasional cathode characterization. All ignitions were normal with no ignition requiring more than the nominal 5 minutes of heating.

In an attempt to measure cathode health over the course of the wear testing, the cathode was periodically operated in diode mode (i.e., with the keeper being the only anode surface). The cathode-keeper current was set to 2.0 A and 2.5 A at three flow rates corresponding to 5%, 7%, and 10% of the wear test anode flow. The keeper voltage decreased by 19% over 500 h for all combinations. However, it is not clear if the change in electrical configuration over this same period affected the results.

F. Back-sputtered Deposition

Figures 17 compares the deposition thickness measured by the 3 QCMs during Segment III of the test campaign. Each QCM collects roughly 0.45 µm over the 360 h which indicates a deposition rate of roughly 1.25 µm/kh. This is consistent with measurement of the deposition thickness on the BN witness plate shown in Fig. 11. Rates measured during the first 400 h of the test campaign (which includes Segment I, II, and 32 h of Segment III) averaged 1.62 µm/kh, or roughly 30% higher than those shown in Fig. 17.[15] The difference is likely due to a combination of significant variations in the TDU operating point in the first 120 hr, higher divergence of higher-energy ions during operation with graphite pole covers, and erosion of new graphite panels in the facility. The back-sputter deposition rate of Segment II alone is estimated to only be 15% higher than Segment III.[15]
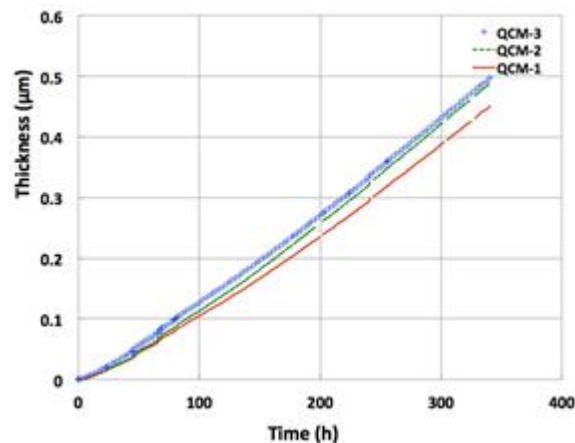

Figure 17. Variation of QCM deposition thicknesses during Segment III.

13

American Institute of Aeronautics and Astronautics

V. Discussion

Data generated during the first three segments of the wear test campaign have provided significant insight in support of the objectives of the wear test campaign presented in Section I.

A. Performance Characterization

Performance data generated during Segment I suggested that design improvements incorporated into TDU-1 have significantly improved its performance.[14] Extended duration testing during Segments II and III have shown that no significant variation occurs over several hundred hours of operation, therefore confirming the sustainability of the performance improvements.

Back-sputter from the facility does not appear to be affecting thruster performance. Additional testing is required to assess whether the buildup of a conducting film on the discharge channel will ultimately impact performance. The measured back-sputter rate of 1.25 µm/kh is roughly one-third that predicted by analytical and numerical codes.[15] These codes are using not only the QCM data, but the various witness plate data provided during the multi-segment test campaign to refine and validate their governing assumptions. The long duration testing will provide unique data to develop these codes and may help to make them a reliable tool for future testing.

B. Wear Measurement

The extended duration testing of the HERMeS TDU-1 has demonstrated that the magnetic shielding design is precluding discharge channel erosion at full power from the initiation of testing. This was predicted based on the preliminary data collected on the earlier version of the TDU,[11] testing of the magnetically shielded H6-MS at JPL,[18] and testing of the magnetically shielded NASA 300-MS at NASA GRC.[23] However, none of these demonstrated zero-erosion of the discharge channel.

The erosion of the graphite inner pole is similar in pattern to that observed on the H6-MS.[18] That thruster was operated at 300 V, 20 A which yielded erosion rates between 40 µm/kh and 60 µm/kh at the inner and outer radii of the inner pole cover, respectively. Rates in the radial center of the inner pole cover were roughly 25 µm/kh. The Mo masks that were incorporated during that test eroded at roughly five times that of the graphite over the radius.[18] Figure 18 compares the Mo, Al_2O_3 and graphite (C) rates for this HERMeS TDU test. Note that the ratio of both Mo and Al_2O_3 to graphite have the same form, with the Mo rates two to three times larger across the radius. From Sekerak,[18] assuming the erosion results solely from singly charged ions, a ratio of 4 suggests that the erosion is caused by ions with energies of 200±50 eV. However, a ratio of 10±2.5 suggests the ions only have energies of 70±30 eV. It has been suggested that the erosion pattern in Fig. 15 results from the electron temperature distribution across the face of the thruster.[24] However, it is also suggested that this distribution does not result in significant radial voltage gradients in the plasma sheath for a conducting pole cover. An alternative explanation would be that the sputter yield of the graphite is relatively insensitive to the variation in ion energies across the radius compared to a factor of 3 increase for Mo and Al_2O_3. Oyarzabal's data[25] suggest this could be the case for Xe II ions with energies between 75 eV and 125 eV impacting the surface over a range of angles. Graphite was shown to sputter preferentially in C_2 and C_3 clusters with total yields varying by less than a factor of two with Xe II angle of incidence below 175 eV. However, Mo yields
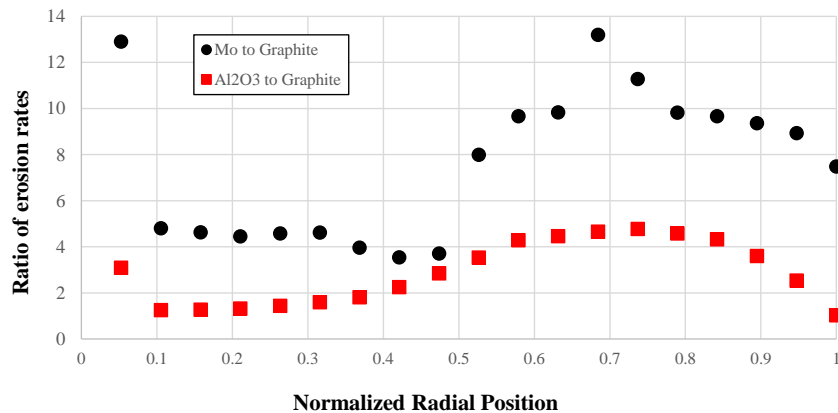

Figure 18. Ratio of measured Mo and Al_2O_3 erosion rates to graphite erosion rates as a function of inner pole cover radius.

American Institute of Aeronautics and Astronautics

varied by up to a factor of 15 with angle of incidence over the same 75-125 eV energy range.[26,27] Exactly opposite trends were reported by Kolasinski which showed a factor of three higher dependence on angle of incidence for graphite than for Mo, albeit at Xe II energies at or above 600 eV.[28] Non-intrusive measurements of plasma properties or further dedicated short duration tests with witness plates of different materials are likely required to resolve the physical mechanism yielding the erosion pattern. However, the similarity in trends shown in Fig. 18, and the relatively good trending with published sputter yields,[26,29] suggests that the difference in erosion rates is primarily a function of material and not of thruster electrical configuration. If the energy of impacting ions doubled in a floating configuration with graphite (as body-to-ground voltage would indicate[22]), then the trend in surface erosion might more closely follow that of Mo and Al_2O_3 shown in Figs. 13 and 15.

The wear pattern measured on the alumina pole cover (Fig. 15) is similar to that observed on the French low-power, magnetically shielded thruster (the PPI).[30] However, the rate for the higher-power TDU is about one-third that observed for the other. This may be a result of the significantly lower background pressure provided by VF-5 despite the 50-fold increase in thruster propellant throughput.

Despite the large (4x) difference in peak erosion rates between alumina and graphite, there is only a 50% difference in volumetric erosion rate. Either pole cover material will likely enable thruster life beyond the 5000 kg throughput requirement of ARRM.[31] The alumina pole cover would have to be proportionally thicker at its point of maximum erosion to enable the same extended life as graphite pole covers of uniform thickness. It is not clear what the limit to this thickness would be, but it would result from a combination of mechanical viability for a sputter deposited ceramic and intrusion into the downstream plasma. No other life limiting mechanism has shown itself to date during the wear testing that would impose a stronger constraint on thruster service life.

C. Initiation of Segment IV of the Test Campaign

The HERMeS TDU-1 entered Segment IV of the test campaign on June 27, 2016, in the configuration shown in Table 2 for a nominal duration of 1272 h. Graphite pole covers are incorporated with graphite masks. Given the detailed erosion measurements made after 246 h, detailed erosion data will be available for discrete durations of 246 h, 1272 h (previously protected regions), and 1518 h (previously exposed regions). The latter two will be measured with respect to the still-protected regions at three azimuthal locations. In addition, a partially polished outer front pole cover with graphite masks will better quantify the erosion near the outer edge of the thruster.

Only minimal performance data will be collected over the duration of Segment IV. This is consistent with Segments II and III which were intended primarily as wear tests. Periodic cathode-only testing will continue and be correlated with an ongoing hollow cathode wear test.[32] The BN discharge channel, hollow cathode assembly, anode, and magnetic circuit will experience the entirety of the 2000 h wear test.

VI. Conclusion

The first 728 h of a nominally 2000 h wear test of the HERMeS TDU-1 have been completed. Data to date have demonstrated that magnetic shielding has eliminated erosion of the BN discharge channel. However, it has introduced erosion of the inner pole cover as seen on other magnetically shielded thrusters. No other life limiting mechanism, such as hollow cathode depletion, has shown itself to date during the wear testing that would impose a stronger constraint.

No significant variations in performance were observed during each of the two wear test segments. Indeed, reference firing conditions conducted over the last 600 h of total operation have shown no variation at lower discharge voltages regardless of pole cover or thruster body electrical configuration (floating or cathode-tied). The impact of back-sputtered material appears to be negligible as well. Coating of the BN discharge channel appears complete and identical-appearing coating on a nearby witness plate shows it to be carbon, roughly 2-μm thick consistent with QCM measurements. No variation in cathode start time or keeper-only operating voltage has been observed.

The first three segments of the overall test were conducted with different front pole covers. Graphite pole covers were incorporated in Segments I and II, though the inner pole cover was different between these two. The thruster was also operated in a novel "cathode-tied" configuration in which the body of the thruster was tied to the cathode which was, of course, isolated from facility ground. Segment III of the wear test ran the more conventional configuration of alumina pole covers with a floating thruster body. The operation of the TDU-1 in a cathode-tied configuration with graphite pole covers appears to offer several advantages over the traditional configuration of dielectric pole covers. These include longer thruster service life for a given pole cover thickness and slightly higher performance. However, both configurations appear capable of meeting the life requirements of ARRM. Additional wear testing is underway to further support the graphite, cathode-tied configuration as a truly viable alternative.

Erosion rates and patterns suggest that the eroding ions have energies less than 125 eV and strike the inner pole surface at varying angles of incidence. This is supported by the common trends of Mo-to-graphite and Al_2O_3-to-graphite erosion rates, and by assuming the graphite preferentially erodes in C_2 and C_3 complexes at low incidence energies. Regardless, in the different configurations the Al_2O_3 has a peak erosion rate four times that of the graphite and a 50 % higher volumetric erosion rate. Optical emission spectroscopy suggests that all erosion rates are constant over the duration of each of the test segments—though, this is to be verified by the ongoing extended duration testing of Segment IV. This fourth and final test segment began on June 27, 2016.

Acknowledgments

References

[1] Smith, B. K., Nazario, M. L., and Cunningham, C. C. , "Solar Electric Propulsion Vehicle Demonstration to Support Future Space Exploration Missions," presented at the Space Propulsion Conference 2012, Bordeaux, France, 2012.

[2] Manzella, D. H. and Hack, K., "High-Power Solar Electric Propulsion for Future NASA Missions," Proceedings of the 50th AIAA/ASME/SAE/ASEE Joint Propulsion Conference, AIAA Paper 2014-3718, Cleveland, OH, 2014.

[3] Kamhawi, H., *et al.*, "Overview of the Development of the Solar Electric Propulsion Technology Demonstration Mission 12.5-kW Hall Thruster," presented at the 50th AIAA/ASME/SAE/ASEE Joint Propulsion Conference, Cleveland, OH, 2014.

[4] Spence, B., *et al.*, "Technology Maturation and Advancement Update of the ROSA/MegaROSA Solar Array," presented at the Space Power Workshop, Huntington Beach, CA, 2014.

[5] Brophy, J. R., and Muirhead, B., "Near-Earth Asteroid Retrieval Mission (ARM) Study," Proceedings of the 33rd International Electric Propulsion Conference, IEPC Paper 2013-82, Washington, DC, 2013.

[6] Gates, M., "NASA's Asteroid Redirect Mission Concept Development Summary," presented at the IEEE Aerospace Conference, Big Sky, MT, 2015.

[7] Muirhead, B. and Brophy, J. R., "Asteroid Redirect Robotic Mission Feasibility Study," presented at the Presented at the IEEE Aerospace Conference, Big Sky, MT, 2014.

[8] Mikellides, I. G., *et al.*, "Magnetic Shielding of a Laboratory Hall thruster. I. Theory and Validation," *Journal of Applied Physics,* vol. 115, no. 4, Jan 28, 2014.

[9] Kamhawi, H., et al., "Performance and Thermal Characterization of the NASA-300MS 20 kW Hall Effect Thruster," Proceedings of the 33rd International Electric Propulsion Conference, IEPC-2013-444, Washington, D.C., October 6-10, 2013.

[10] R. R. Hofer, *et al.*, "Magnetic shielding of a laboratory Hall thruster. II. Experiments," *Journal of Applied Physics,* vol. 115, no. 4, Jan 28, 2014.

[11] Kamhawi, H., *et al.*, "Overview of the Development of the Solar Electric Propulsion Technology Demonstration Mission 12.5-kW Hall Thruster," Proceedings of the Proceedings of the 50th AIAA Joint Propulsion Conference, AIAA Paper 2014-3898, July, 2014.

[12] Hofer, R. R., *et al.,* "Development Risks and Design of the 12.5 kW HERMeS Hall Thruster for the Solar Electric Propulsion Technology Demonstration Mission," 62nd JANNAF Propulsion Meeting, June, 2015.

[13] Brophy, J., "Near-Earth Asteroid Retrieval Mission (ARM) Study," Proceedings of the 33rd International Electric Propulsion Conference, IEPC Paper 2013-082, October, 2013.

American Institute of Aeronautics and Astronautics

[14] Kamhawi, H., *et al.*, "Performance and Stability Characterization Tests of NASA's 12.5-kW Hall Effect Rocket with Magnetic Shielding Thruster," Proceedings of the 52nd Joint Propulsion Conference, AIAA Paper 2016-4826, July, 2016.

[15] Gilland, J. H., Williams, G. J., Burt, J. M., and Yim, J., "Carbon Back-Sputter Modeling for Hall Thruster Testing," Proceedings of the 52nd Joint Propulsion Conference, AIAA Paper 2016-4941, July, 2016.

[16] Kamhawi, H., *et al.*, "Performance Characterization of the Solar Electric Propulsion Technology Demonstration Mission 12.5-kW Hall Thruster," Proceedings of the 34th International Electric Propulsion Conference, IEPC Paper 2015-007, Kobe, Japan, July, 2015.

[17] Shastry, R., and Soulas, G., "Post-test Inspection of NASA's Evolutionary Xenon Thruster Long-Duration Test Hardware: Discharge and Neutralizer Cathodes," Proceedings of the 52nd Joint Propulsion Conference, AIAA Paper 2016-4631, July, 2016.

[18] Sekerak, M. J., Hofer, R. R., Polk, J. E., Jorns, B. A., and Mikellides, I. G., "Wear Testing of a Magnetically Shielded Hall Thruster at 2000 s Specific Impulse," 34th International Electric Propulsion Conference, IEPC Paper 2015-155, July, 2015.

[19] Williams, G., J., and Kamhawi, H., "Optical Characterization of Component Wear and Near-field Plasma of the HERMeS Thruster," 62nd JANNAF Propulsion Meeting, June, 2015

[20] Cho, S., *et al.,* "Hall Thruster Channel Wall Erosion Rate Measurement Method Using Multilayer Coating Chip," Proceedings of the 46th AIAA Joint Propulsion Conference, AIAA-2010-6697, Nashville, Tennessee, July 2010.

[21] Cremer, R., *et al.*, "Sputter deposition of crystalline alumina coatings," Surface and Coatings Technology Vol 163-164, January 2003, pp157-163.

[22] Peterson, P. Y., *et al.*, "NASA HERMeS Hall Thruster Electrical Configuration Characterization," Proceedings of the 52nd Joint Propulsion Conference, AIAA Paper 2016-5027, July, 2016.

[23] Kamhawi, H., Haag, T. W., Huang, W., and Hofer, R. R., "The Voltage-Current Characteristics of the 12.5 kW Hall Effect Rocket with Magnetic Shielding at Different Background Pressure Conditions Presented at the 62nd JANNAF Propulsion Meeting, Nashville, TN, 2015.

[24] Mikellides, I., Hofer, R. R., Katz, I., and Goebel, D. M., "Magnetic Shielding of Hall Thrusters at High Discharge Voltages," *Journal of Applied Physics,* vol. 116, 2014 2013.

[25] Oyarzatal, E., "Molybdenum and Carbon atom and carbon cluster sputtering under low-energy noble gas plasma," Ph.D. Dissertation, Engineering Physics, University of California, San Diego, 2008.

[26] Oyarzabal, E., *et al.*, "Molybdenum and Carbon Cluster Angular Sputtering Distributions Under Low-Energy Xenon Ion Bombardment," Proceedings of the 41st AIAA Joint Propulsion Conference, AIAA Paper 2005-3525, July, 2005.

[27] Williams, J. D., Johnson, M. L., and Williams, D. D., "Differential Sputtering Behavior of Pyrolytic Graphite and Carbon-Carbon Composite Under Xenon Bombardment," Proceedings of the 40th AIAA Joint Propulsion Conference, AIAA Paper 2004-3788, July, 2004.

[28] Kolasinski, R. D., Polk, J. E., Goebel, D., and Johnson, L. K., "Carbon Sputtering Yield Measurements at Grazing Incidence," Proceedings of the 42nd AIAA Joint Propulsion Conference, AIAA Paper 2006-4337, July, 2006.

[29] Tartz, M., Heyn, T., Bundesmann, C., and Neumann, H., "Measuring sputter yields of ceramic materials," Proceedings of the 31st International Electric Propulsion Conference, IEPC Paper 2009-240, September 2009.

[30] Grimaud, L., "Design and characterization of a 200 W low power Hall thruster in "Magnetic Shielding" and "wall less" configurations," 2016 Space Propulsion Conference, Paper 3124890, May, 2016.

[31] Herman, D., et al., "The Ion Propulsion System for the Asteroid Redirect Robotic Mission," Proceedings of the 52nd Joint Propulsion Conference, AIAA Paper 2016-4824, July, 2016.

[32] Verhey, T. et al., "Hollow Cathode Assembly Development for the HERMeS Thruster," Proceedings of the 52nd Joint Propulsion Conference, AIAA Paper 2016-5026, July, 2016.

American Institute of Aeronautics and Astronautics